FULL PAPER

DOI: 10.1002/cjoc.201300843

All-Atom Molecular Dynamics Simulation of Structure and Diffusion of Hydrophilic Antistatic Agents in Polypropylene

Lianhua Long, Yingzi Yang, and Feng Qiu*

State Key Laboratory of Molecular Engineering of Polymers, *Department of Macromolecular Science*, *Fudan University*, *Shanghai 200433*, *China*

Glycerol monostearate (GMS) is an additive widely used in plastic industry for its good ability to improve the wettability and antistatic property of polymer surfaces. Based on GMS, we propose five additives of different polarity by attuning the number of oxyethyl groups. All-atom molecular dynamics simulations of these additives in polypropylene (PP) matrix are carried out at temperatures of 300 K, 350 K and 400 K. Detailed molecular conformations are obtained and analyzed. Due to the gauche effect of the dihedral angles, the polar parts of these additives form helix structures. The diffusion coefficient of the additives depends on their molecular conformations and decreases monotonously with increasing polarity. These results are expected to be helpful in rational design of hydrophilic antistatic agents in polymeric materials.

Keywords antistatic additive, glycerol monostearate, polypropylene, diffusion, molecular dynamics

Introduction

Polymers are easy to accumulate electrostatic charges due to low dielectric constant and high surface electrical resistance. Sometimes polymeric materials even suffer a high electrostatic charge up to 1.5×10^4 V due to low moisture degree in air, rubbing and dust.[1] The high electrostatic charge brings problems to the processing procedure, the appearance of the product, and the scope of application of polymer materials, and even causes fire or explosion. Therefore, it is very crucial to avoid unfavorable accumulation of static electricity. One of the effective methods is blending antistatic additives within polymers to increase the surface electrical conductivity and the dissipation rate of the electrostatic charge.

Antistatic additives are generally categorized into the external and the internal ones. The external antistatic additives are directly applied on the surface of polymer materials, while the internal antistatic additives are added within polymer matrix during the preparation process. The internal antistatic agents are suitable for commercial application, because they build a conductive path for the dissipation of electrostatic charges with relatively homogeneous and stable electrical properties.[1] Inorganic fillers, conductive polymers, hydrophilic molecules are usually used as internal antistatic agents.

Compared with inorganic fillers and conductive polymers, hydrophilic antistatic additives do not significantly change the pristine color of polymer matrix.[2] Generally, a hydrophilic additive molecule has a hydrophilic group building the conductive path, and a hydrophobic group immersed within the polymer matrix. Through the mixing process, the hydrophilic additives form a network, resulting in effective pathways throughout the polymer matrix to disperse accumulated electrostatic charges.[2] In addition, the hydrophilic groups emerged on the surface absorb more moisture from the surrounding air, and thus reduce the surface electrostatic charges.[1]

The efficiency of antistatic agents is determined by a serial of additive and matrix properties, such as the molecular weight of antistatic agent molecules, the surface tension gradient, and the surface roughness of polymer matrix.[3-5] Among these, the migration rate of molecules is especially important for the lifetime of antistatic agents. Small molecules with controllable migration rate have attracted intensive research due to their abundant applications including packaging,[6,7] additive migration,[8-11] gas separation,[3,12-14] osmosis,[14] biosensors,[15] drug releases,[16,17] and ion exchange.[18] However, when the molecules are immersed in a polymer matrix, direct measurement of the migration rate is difficult due to very long time scales of diffusion.[19,20]

In order to solve this problem, Limm *et al*.[21] and Brandsch *et al*.[22] developed semi-empirical models to calculate the migration rate of non-polar fatty molecules in polyolefins. They pointed out that the diffusion rate depends on a series of factors such as polymer crystallinity,[23] antistatic molecular concentration, tempera-

* E-mail: fengqiu@fudan.edu.cn
Received November 22, 2013; accepted February 10, 2014; published online March 5, 2014.

CHINESE JOURNAL OF CHEMISTRY

ture,[21] and chemical compatibility between the antistatic agent and the polymer. Employing a series of assumptions, their semi-empirical models can predict the diffusion rate of simple molecules, such as the diffusion rate of non-polar fatty molecules in polyolefins.[24] However, this semi-empirical models is limited to deal with molecules of complex structures.

It is found that the molecular conformation and polarity are very important to diffusion and other physical properties of additives in a polymer matrix. A systematic study on the influence of molecular conformation on migration rate indicated that the long, flexible alkyl chains are crawling based on the large degrees of freedom, while the rigid molecules jump.[25] In case of the alkane isomers dispersed in polymer matrix, the methyl branches decrease the collision diameter and lead to larger diffusion coefficients than linear alkanes.[26] Polar molecules added within polypropylene (PP) matrix tend to segregate on material surface, with a surface concentration strongly depending on their diffusion rates in PP matrix.[27] However, due to complex molecular structures and diverse chemical compatibilities, the understanding of how the molecular polarity influences the mobility of the antistatic agents in polymer matrix is still far from enough.

Glycerol monostearate (GMS) used in polyolefins is widely known as an immediate performance antistatic agent but with short duration only about one month.[28] Based on GMS, we propose a series of derivative molecules with different polarity by changing the number of oxyethyl groups and keeping the molecular length unchanged. In fact, the study on hydrophilic migratory additives in PP films has pointed out the influence of the polarity on the diffusion coefficient remaining a problem to be solved.[20]

Recent advances in molecular dynamics (MD) simulations render their application in calculating the migration rate of organic molecules with a high degree of precision.[24] The greatest advantage of MD is that it gives a direct view of the dynamic conformation of molecules, which elucidates the relation between molecular structure and diffusion better. Therefore, MD is now widely used to investigate the dynamics of polymer systems.[29-36] Moreover, the force field, which is central to the accuracy of MD, has been proved to be accurate for PP.[10,20,37,38]

Therefore, in this paper, we carry out MD simulations to study the single molecular conformation and dynamics of GMS-derived additives dispersed in a chemically incompatible PP matrix. In Section II, we briefly introduce the MD simulation method and the details of the simulation settings. In Section III, we analyze the simulation data and discuss how the polarity affects the molecular conformation of the additives and consequently influences their mobility. In the last section, we summarize our conclusions.

Molecular Dynamics Method

In this work, Large-scale Atomic/Molecular Massively Parallel Simulator (LAMMPS) code was used.[39] The MD simulations were performed at different temperatures ranging from room temperature to the maximum use temperature for PP (300 K, 350 K and 400 K) in the canonical ensemble (NVT) except the annealing procedure which adopted isothermal-isobaric ensemble (NPT). The NVT ensemble temperature was controlled by a Nose-Hover thermostat with a relaxation time of 0.1 ps.[40] The Reversible Reference System Propagator Algorithms (RESPA) were used to predict the motion state of the particles with a time step of 1fs.[41] The periodic boundary condition was employed. The simulation results were visualized by Visual Molecular Dynamics (VMD).[42]

Force fields

The MD simulations were carried out with the Optimized Parameters for the Liquid Simulation-All Atom (OPLS-AA) force field.[43] Among different force fields, diffusion coefficients calculated via OPLS agree better with the experimental results.[44] OPLS-AA force field was calculated via four types of potentials: bond potential, angle stretching potential, torsion potential and non-bonded interactions potential.[45,46] The inner and outer cutoff of the distance between two atoms for the calculation of non-bonded interactions potential were 0.8 nm and 1 nm, respectively. A distance cutoff was not used for the long Coulomb interactions since they were calculated using the particle-particle/particle-mesh (PPPM) algorithm.[47]

Sample preparation

Based on the molecular structure of GMS, we proposed a series of similar additives with the same molecular chain length and comparable molecular weight by substituting the $-CH_2-CH_2-CH_2-$ group by the more polar oxyethyl group ($-CH_2-CH_2-O-$). We use G-C_nE_m to denote the molecular structure, where "G" means the derivatives based on GMS, and n and m denote the number of $-CH_2-CH_2-CH_2-$ and oxyethyl groups in the molecule, respectively (as shown in Figure 1). The variation of the number of oxyethyl group allows a fine control on the hydrophobic-lipophilic balance (HLB) of the molecules. The HLB value, determined by Griffin method,[48] increases monotonously with increasing oxyethyl number, corresponding to increasing polarity of the molecules. The HLB value from 0 to 20 corresponds to the molecular polarity from completely lipophilic to completely hydrophilic. Therefore, the HLB value of GMS-like additives increases with the increasing ratio of the polar part.

The system was built as follows. First, we randomly built 40 polypropylene (PP) chains without relaxation, using radical-like polymerization but fixing the polymer's tacticity.[49] Each PP chain consisted of 50 repeat units including totally 452 atoms. Then we added five

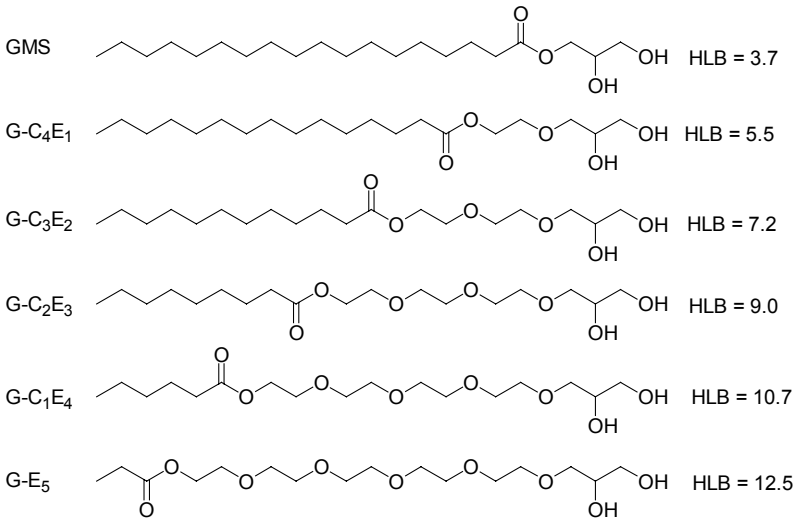

Figure 1 The chemical structures and the hydrophobic-lipophilic balance (HLB) values of glycerol monostearate (GMS) and its derivatives G-C_4E_1, G-C_3E_2, G-C_2E_3, G-C_1E_4 and G-E_5.

GMS-like molecules into the system by setting their chain ends on different positions with large enough distance between each other to avoid any interaction between them during the simulation. The density of the initial packing cell was set to be 0.857 g/cm^3, which is the density of the amorphous PP. After energy minimization, the system experienced an annealing procedure which heated the system from 300 K to 500 K with an interval of 50 K and then cooled down from 500 K to the settled temperatures (300 K, 350 K or 400 K) with an interval of 50 K. At each temperature stage, a 100 ps NPT dynamics was carried out on the cells. Afterwards, a 100 ps NPT (settled temperature, 10^5 Pa) MD run was performed to obtain the equilibrium density. Finally, 4 ns NVT dynamics was performed to approach equilibrium state. The subsequent analysis lasted for 16 ns for 300 K and 400 K, 170 ns for 350 K. The atomic trajectory was recorded every 10 ps, and the center of mass (COM) of each molecule was recorded every 500 fs. Figure 2a shows a snapshot of the system including 40 PP chains and five G-E_5 molecules in equilibrium state. In order to obtain an adequate sampling of molecular conformations, we carried out five runs for each system with different random numbers for the initial state, and in each run five additive molecules are added. Thus our statistics of one additive is based on 25 molecules each with movement lasting at least 16 ns, which we believe is enough for the molecular conformation analysis.

Results and Discussion

In order to understand how the additive molecules behave to cope with the chemical incompatible environment, the conformation of the molecules, the movability of atoms, and the diffusion coefficient of each additive are analyzed.

For each molecule, we choose the carbon atom of the ester group as the reference one whose polarity is positive most (as shown in Figure 2(b)), and set the serial number of the reference atom as zero. The serial number is negative for the atoms in the nonpolar tail, and is positive for the atoms in the polar head. The position of atom i on the backbone of the molecule is $\boldsymbol{R}_i$. We define the local unit tangent vectors $\boldsymbol{\tau}_i = \boldsymbol{r}_i/|\boldsymbol{r}_i|$, where $\boldsymbol{r}_i = \boldsymbol{R}_i - \boldsymbol{R}_{i-2}$.

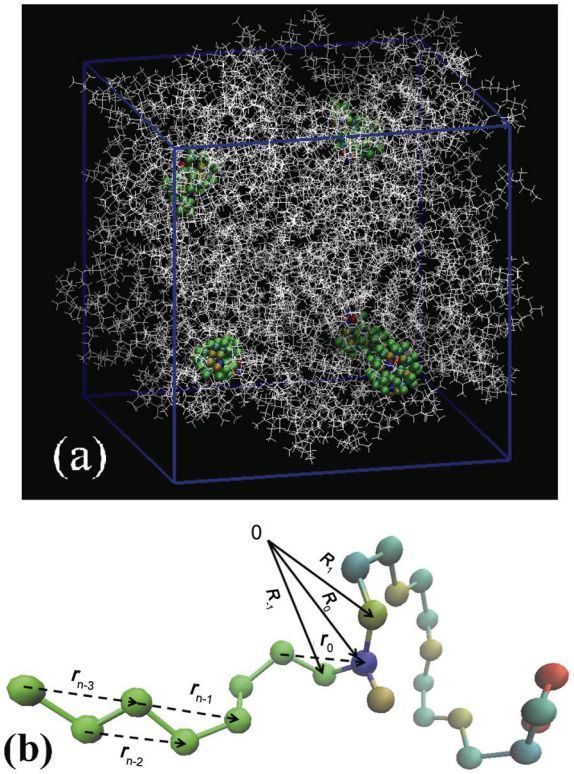

Figure 2 (a) A snapshot of the whole system with PP chains (white lines) and five G-E_5 molecules (color spheres). (b) Vectors of the atoms ($\boldsymbol{R}_i$) and the vectors between atoms ($\boldsymbol{r}_{n-i}$) of G-C_2E_3 (the hydrogen atoms are not shown). The colors from red to green to blue represent the polarity of the atoms from negative most to neutral to positive most.

CHINESE JOURNAL OF CHEMISTRY

Molecular conformation

Molecular conformation has significant correlation to the chemical and physical properties, such as molecular mobility, chemical activity of atoms and groups, *etc*.[33]

The snapshots of instantaneous conformation of GMS and its derivatives are shown in Figure 3. Obviously, due to the distinct chemical property, the polar heads and the nonpolar tails of the additive molecules exhibit different conformations. The nonpolar tails of each molecule adopt extended conformations like freely rotating chain, except the nonpolar tail of G-E_5 which is too short. However, the polar heads employ distorted and shrinking structures.

In order to reveal the details of the additives' conformation, we analyze the distance between the atoms, the orientation correlation functions, and the dihedral angles.

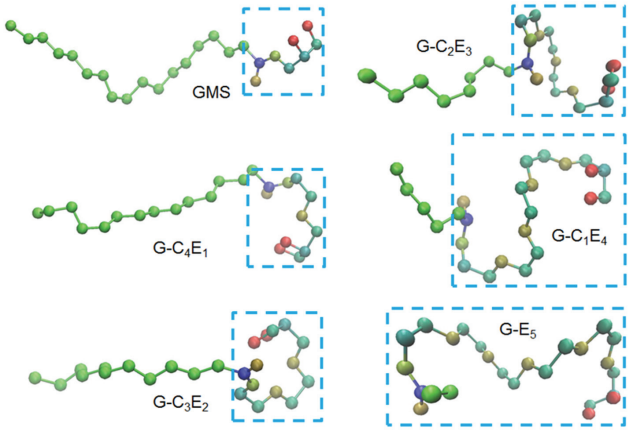

Figure 3 Conformations of the additive molecules dispersed in PP matrix under 300 K (hydrogen atoms are not shown). The colors from red to blue represent the polarity of the atoms from negative most to positive most. The boxes with dashed-lines indicate the hydrophilic part of the additive molecules.

Average distance between atoms

The distance between the atoms in a same molecule, especially the end-to-end distance, is used to characterize the stretching and compression of the chain-like molecules. The time-averaged distance D_{i0} between atom i and the reference atom in the same molecule is defined as,

$$D_{i0}=\left\langle \left| \boldsymbol{R}_i-\boldsymbol{R}_0 \right| \right\rangle_t \tag{1}$$

As shown in Figure 4, for both nonpolar tails ($i<0$) and polar heads ($i>0$), D_{i0} increases with the serial number difference. But the slope of the lines for the polar heads is much smaller than that for non-polar tails, indicating the compressed polar heads and the stretched non-polar tails. Moreover, the distance of the oxygen on the polar heads ($i=4$, 7, 10, 13, 16) is always smaller than their adjacent atoms, which suggests a hidden fine structure in the compressed polar head.

To elucidate the structure of the polar heads, we further analyze the main chain orientation correlation and the dihedral angles of the additive molecules.

Orientation correlation function

The orientation correlation function of the main chain of the molecule is defined as,

$$g_i=\left\langle \boldsymbol{\tau}_i \cdot \boldsymbol{\tau}_0 \right\rangle \tag{2}$$

where $\boldsymbol{\tau}_0$ is the tangent vector pointing to the reference atom.

As shown in Figure 5a, $g(i)$ for the non-polar tails of different additives almost overlaps with each other. Indeed, for GMS with the longest nonpolar tail (Figure 5a), $g(i<0)$ exhibits a simple, monotonously decreasing with decreasing i. The root of the mean-square deviation of $g(i<0)$ of GMS increases as i decreases, which reflects the losing orientation correlation with the increasing contour distance from the reference vector. Although the nonpolar part of GMS is not long enough to exhibit the vanish of $g(i)$ for infinite i, we can estimate the persistent length as approximately 10 carbon bonds according to the decreasing rate of $g(i)$.

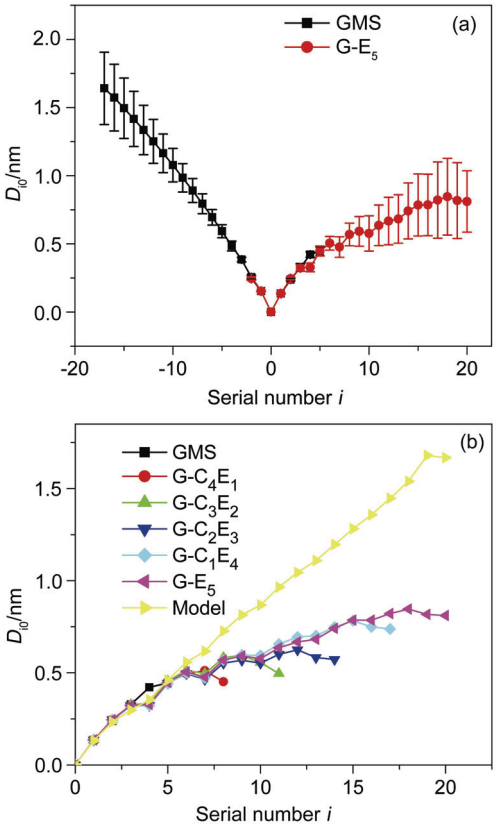

Figure 4 The average distance D_{i0} between the ith atom on the molecular backbone and the reference carbon atom of ester group at 300 K. (a) D_{i0} of GMS and G-E_5 with error bars. (b) D_{i0} for the polar heads ($i>0$) of GMS, G-C_4E_1, G-C_3E_2, G-C_2E_3, G-C_1E_4, G-E_5 and the model built in Figure 7.

In contrast to the monotonous behavior of $g(i<0)$ for non-polar tails, $g(i>0)$ for the polar heads shows much more complicated structure with three notable characters, a sharp decreasing part connecting non-polar tails region, an obvious undulation around zero, and the step-like plateaus consisting of three successive data points, as shown in Figure 5b.

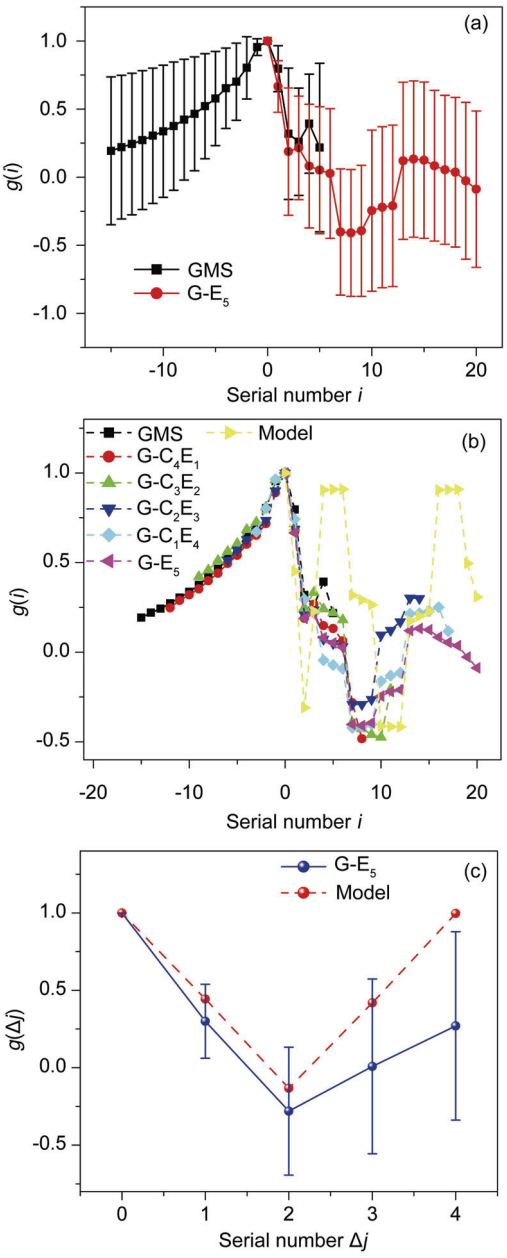

Figure 5 The orientation correlation function $g(i)$ at 300 K. (a) $g(i)$ of GMS and G-E_5 with standard deviations represented as error bars. (b) $g(i)$ of GMS, G-C_4E_1, G-C_3E_2, G-C_2E_3, G-C_1E_4 , G-E_5 and the model built in Figure 7. (c) The angle correlation functions of the orientation unit vectors of -C-O-C- segments in G-E_5 and the model built in Figure 7.

For $0\leqslant i\leqslant 2$, $g(i)$ almost overlaps for all GMS derivatives. It decreases sharply from 1 to approximately 0.25, indicating the main chain orientation rotates for approximately $11\pi/12$ within the molecular fragment -C-C-C-O-C- (which connects the non-polar tail and the polar head).

The undulation of $g(i>0)$ indicates that the polar heads embedded in the chemically incompatible PP matrix have a periodic structures. Although $g(i>0)$ for different molecules do not overlap as well as $g(i<0)$ do, they share a similar variation trend, such as the minimum at $i=(7, 8, 9)$ and the maximum at $i=(13, 14, 15)$. Theoretically, $g(i)$ should approach zero with increasing i due to the finite rigidity of the chain molecule and the non-zero temperature $\kappa_B T$. However, we cannot see the decaying undulation amplitude of $g(i>0)$ even for G-E_5. We attribute this to the polar part being too short to exhibit the effect of thermal fluctuation. The undulation of $g(i<0)$ indicates a repeating structure along the main chain. The period of such structure is approximately 12 bonds, determined by doubling the distance between the vale and the peak of $g(i>0)$.

The orientation correlation of polar heads shows a series of step-like structures consisting of three successive data points. The number of the steps equals to the number of oxyethyl groups. The three successive vectors ($\boldsymbol{r}_{n-1}$, $\boldsymbol{r}_{n-2}$, $\boldsymbol{r}_{n-3}$) should correlate the spacial positions of five atoms (see Figure 2). Such a phenomenon indicates that the vectors are on the conical surface of a right circular cone with the reference vector as the axis, or the vectors are parallel to each other. However, we cannot differentiate these two cases from $g(i)$. Therefore, in next subsection, we analyze the dihedral angles in order to observe the relative position of neighboring atoms of oxyethyl groups.

We denote the local tangent vector calculated via two carbon atoms neighboring to the oxygen atom as $\boldsymbol{\tau}'_j$, which represents the local direction of -C-O-C- segment. Therefore, $\boldsymbol{\tau}'_j=\boldsymbol{\tau}(3j+2)$, $j=1, 2, \cdots, m$, where m is the serial number of -C-O-C-. The direction correlation of oxyethyl group is,

$$g(\Delta j)=\langle \boldsymbol{\tau}'_{j_1}\cdot\boldsymbol{\tau}'_{j_2}\rangle_t, \Delta j=|j_1-j_2| \quad (3)$$

We calculated the angle correlation function of -C-O-C- orientation vectors of G-E_5 at 300 K, as shown in Figure 5c. $g(\Delta j)$ first decreases then increases with Δj, indicating a local structural correlation between all -C-O-C- fragments on G-E_5. The correlation decays because the molecule is not totally rigid. A minimum value exists at $\Delta j=2$ which is the angle of the selected plane and the second plane counted from either direction.

Dihedral angle

Dihedral angle describes the relative position of four atoms. The dihedral angles can be gauche (G) or trans (T).[50,51] Figure 6 shows the distribution functions of three successive dihedral angles -C-O-C-C-, -O-C-C-O-, and -C-C-O-C- of G-E_5 at 300 K. In Figure 6a, the dihedral distribution functions of -C-O-C-C- and

-C-C-O-C- exhibit a strong peak at π, and two faint peaks at π/3 and 5π/3, which indicates the dominant T conformation. Therefore, the five atoms -C-C-O-C-C- locate almost on a flat plane. Combining the dihedral distribution functions with the orientation correlation function shown in Figure 5, we conclude that the three vectors on the same "step" in Figure 5 are parallel to each other. In contrast, as shown in Figure 6b, the dihedral of -O-C-C-O- has a large possibility taking G conformation, but has much smaller possibility for T conformation. The statistics of the dihedral angles of G-E_5 show that the possibility of seeing the combination of three dihedral angles TTT, TTG, TGT, TGG, GTT, GTG, GGT and GGG are 0.020, 0.006, 0.868, 0.044, 0.001, 0.001, 0.058 and 0.001, respectively. Note the significantly high possibility of TGT conformation, which means the molecule takes absolute majority time staying in this state. The small possibility of other conformation is understood as strong environmental fluctuations happened to break TGT structure temporally. This TGT conformation phenomenon is named gauche effect which was also seen in 1,2-dimethoxyethane, 2-methoxyethanol,[51] and poly(oxyethylene) chain in aqueous.[50] Usually TTT is the one with the lowest barrier energy in vacuum. But in solution, TGT's percentage is usually higher.[50,51]

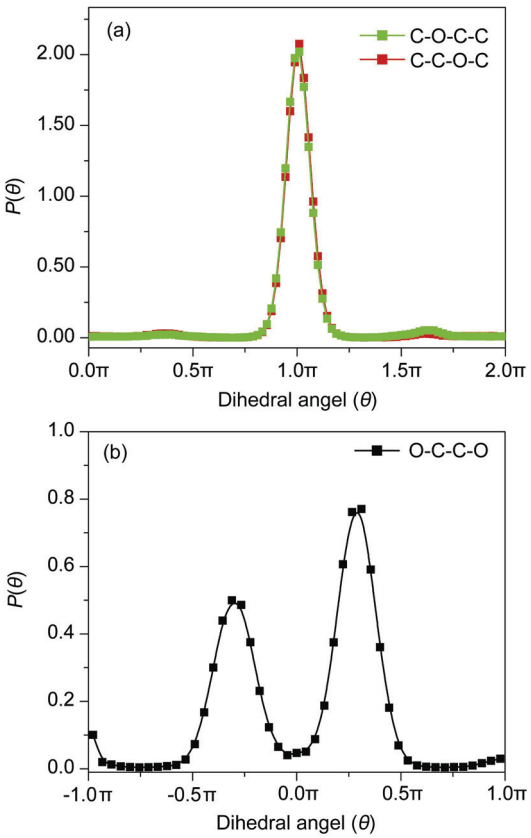

Figure 6 The dihedral distribution functions of (a) C-O-C-C, C-C-O-C and (b) O-C-C-O of G-E_5 at 300 K.

Molecular conformation model

According to the dominant TGT sequence of the three successive dihedral angles -C-O-C-C-, -O-C-C-O-, and -C-C-O-C-, we are able to build a model of G-E_5, as shown in Figure 7. The bond length and angle between the atoms are given by their equilibrium values in OPLS force field. The dihedral angels are built as follows. For dihedrals related to -C-C-O- segments, we use standard TGT conformation, *i.e.* dihedrals of -C-O-C-C-, -O-C-C-O- and -C-C-O-C- are π, π/3 and π, respectively. Note that the dihedral of -O-C-C-O- also has high possibility at −π/3. We only use one value for dihedral of -O-C-C-O- here to simplifying construction of the model since the fractions of the -O-C-C-O- dihedral conformation with either π/3 or −π/3 are approximately the same. For other dihedrals, we use the statistical data based on the simulation.

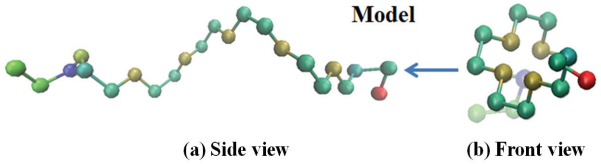

Figure 7 (a) The side view of the G-E_5 model, and (b) the front view of (a) from the direction showed by the arrow. The colors from red to blue represent the polarization of the atoms from negative most to positive most.

The repeating of TGT conformation results in a helix structure. The front view of the model (Figure 7a) shows that the polar part of -C-C-O- segments forms a helix. From the side view (Figure 7b), it looks like a 4-crown ether. The angle correlation function of -C-O-C- orientation vectors for this model has a maximum value at $\Delta j=4$ (Figure 5c), which indicates that four -C-C-O- segments form a period of the helix structure.

We compare the distance D_{i0} for the model with the simulation results as shown in Figure 4b, and find that the slope of the polar part for the model is larger and the drop of the oxygen atom is less obvious. This difference indicates that G-E_5 in PP matrix is more compressed than the model shows.

We attribute the compressed helix configuration to the chemical incompatibility between the polar heads and non-polar PP matrix. The polar heads tend to collapse and aggregate closely to decrease the unfavorable contact energy between them and the surrounding PP. The oxygen atoms, which have the strongest electronegativity, are wrapped near the center of the helix structure by the neutral carbons. Therefore, the interaction energy between the additive and the PP bulk is minimized. Moreover, the flexibility of the C—O bonds enables the rotation of the atoms connected with them much easier.

Atom movability

The movability of atoms depends on not only atomic numbers but also the configuration of molecules, the exact position of the atoms, and chemical environment.[52] In order to analyze the atom movability, we calculate the root-mean-square fluctuation (RMSF) within 3 ns time interval of each atom on the molecular backbone, as shown in Figure 8.

The oxygen atoms on the molecular backbone have two connected neighboring atoms. Therefore, their steric hindrance is smaller than the carbon atoms which have four connected neighboring atoms. Under this situation, the oxygen will choose favorable conformation with lower energy. Figure 8 shows the mobility of the oxygen atoms in -C-O-C- groups of G-E_5 is much lower than the carbon atoms on the molecular backbone. The low movability of the oxygen atoms also supports the helix conformation of the molecule—the oxygen atoms always stay in the inner side of the helix where the available free space is very limited.

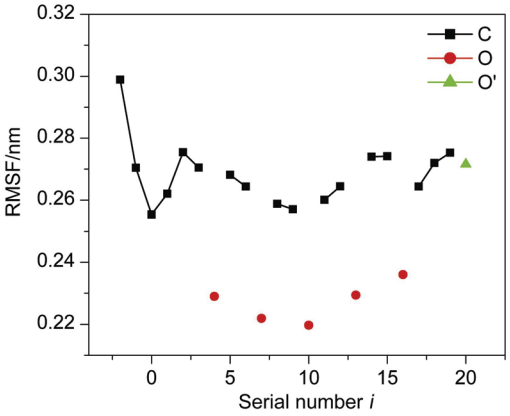

Figure 8 The RMSF of the atoms of G-E_5 at 300 K. The black squares and the blue triangles represent the carbon atoms and the oxygen atoms of hydroxyl group in the molecular backbone, respectively. The red circles represent the oxygen atoms of the oxyethyl groups.

Diffusion coefficient

Based on the detailed knowledge of the molecular conformation of GMS and its derivatives, it is possible to correlate the molecular conformation with the molecular movability that corresponds to its diffusion coefficient in PP matrix.

For all aditives, at 400 K the root-mean-square displacement (RMSD) is less than 7 nm for 16 ns (approximately 4.4 nm on average). Since the root-mean-square radius of gyration (RMSRG) of the molecule is about 0.7 nm, the displacement is barely enough to investigate the long term diffusion properties. At 350 K we prolonged the simulation time to 170 ns and obtained the average RMSD for each additive larger than 4.4 nm. However, at 300 K the RMSD is only 0.5 nm for 16 ns. At least 3000 ns is needed for the RMSD to reach ten times of the molecule RMSRG in order to accumulate convincible data, which is far beyond our present calculation capacity.

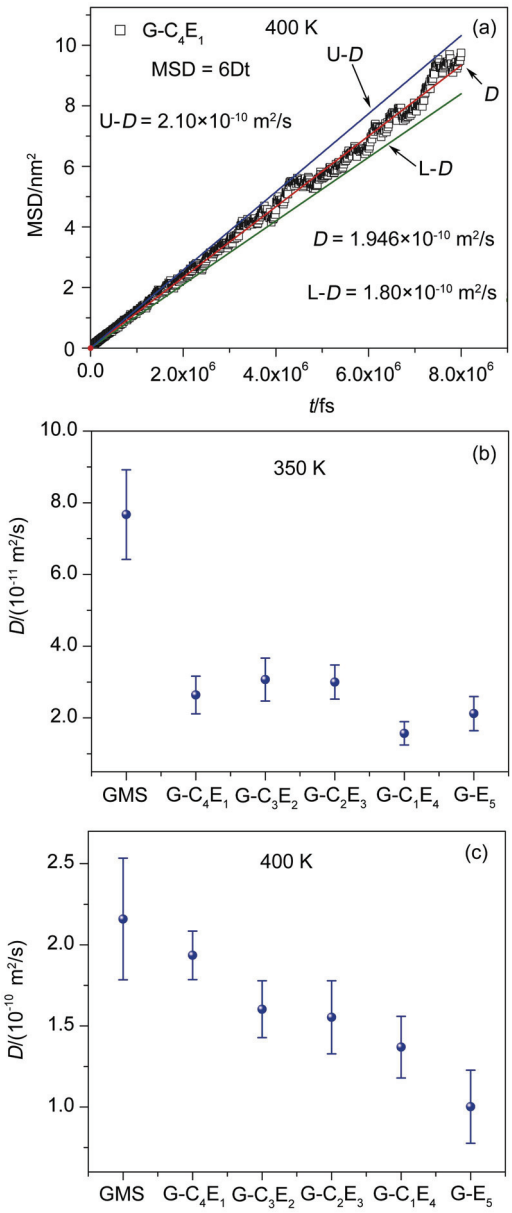

Figure 9 (a) Mean-square displacement vs. time for G-C_4E_1 at 400 K; (b) and (c) are the diffusion coefficients of GMS, G-C_4E_1, G-C_3E_2, G-C_2E_3, G-C_1E_4 and G-E_5 in the PP matrix at 350 K and 400 K, respectively. The error bars are given by the slopes of two enveloping lines, for example, dashed lines as shown in (a).

The diffusion coefficient is calculated by the linear fitting of RMSD with respect to time. In order to estimate the error bar of the diffusion coefficient, we calculate two slopes U-*D* and L-*D*, which are the upper and lower enveloping lines of the data, respectively, as shown in Figure 9a. The difference of U-*D* and L-*D* is defined as the width of the error bar of the diffusion coefficient.

The diffusion coefficients of GMS and its derivatives at 350 K and 400 K are shown in Figure 9b and Figure 9c. GMS is always the one with the highest diffusion coefficient, 7.7×10^{-11} cm^2/s at 350 K and 2.2×10^{-10}

cm^2/s at 400 K, which we attribute to the longest hydrophobic tail having the best compatibility with the PP matrix. At 400 K, the diffusion coefficients exhibit a monotonous decrease with the number of oxyethyl groups increasing in GMS derivatives. However, at 350 K, all GMS derivatives have much lower diffusion coefficients than GMS, and these values do not show obvious dependence on the number of oxyethyl groups. We speculate that at higher temperature (400 K), due to the frequent disassemble of the helix structure, the chain-like, flexible additive molecules crawl through the network of PP chains to diffuse. In this case, the chemical incompatibility dominates the diffusion rate while the chain conformation is less important. However, at lower temperature (350 K), the helix structure, which behaves like a rigid, compressed body, employs the jumping mode for diffusion.[25] Therefore, the diffusion coefficient of GMS derivatives depends strongly on the size and shape of the compressed polar head, except for GMS which has too small polar head to block the crawling motion of the non-polar tail.

Conclusions

We have employed all-atom molecular dynamics simulation to investigate the conformation behaviors of antistatic agents in PP matrix. We proposed five hydrophilic antistatic agents based on GMS by substituting $-CH_2-CH_2-CH_2-$ by $-CH_2-CH_2-O-$. And according to the number of $-CH_2-CH_2-CH_2-$ and $-CH_2-CH_2-O-$ in the molecules, we named them G-C_4E_1, G-C_3E_2, G-C_2E_3, G-C_1E_4 and G-E_5. Including GMS, we investigated six additives with increasing numbers of oxyethyl groups.

In order to elucidate the typical molecular conformation, we carefully analyzed the average atom distance D_{i0}, the angle correlation functions $g(i)$, and the dihedral angle distribution of C-O-C-C, O-C-C-O and C-C-O-C of G-E_5 at 300 K. We find that in PP matrix the polar part of the additives prefers a repeating trans, gauche, trans sequence (TGT) for three successive dihedral angles of C-O-C-C, O-C-C-O and C-C-O-C, leading to a helix structure with a period of approximately four -C-O-C- segments. Such a helix structure is compressed in the chemically incompatible PP matrix, wrapping all oxygen atoms inside the helix to reduce the interaction energy with PP. Therefore, although the C—O bond is flexible to rotate, the movability of the oxygen atom in -C-O-C- segment is always much lower than its neighboring carbon atom due to much less free space inside the helix structure.

The diffusion coefficient of all the additives shows a monotonous decrease with increasing number of oxyethyl groups at 400 K, while it does not obviously related to the molecular hydrophilic property at 350 K. We speculate that both the molecular conformation and the chemical property play important roles on the molecular diffusion behavior. However, more simulation works in the future are necessary to reveal the hidden relation.

Acknowledgement

We gratefully acknowledge the financial support from the National Basic Research Program of China (No. 2011CB605700) and National Natural Science Foundation of China (No. 21320102005). Y. Yang gratefully acknowledges support from the China Postdoctoral Science Foundation (No. 20100480558).

References

[1] Costa, J. C.; Oliveira, M.; Machado, A. V.; Lanceros-Méndez, S.; Botelho, G. *J. Appl. Polym. Sci.* **2009**, *112*, 1595.
[2] Grob, M. C.; Minder, E. *Plast. Addit. Compounding* **1999**, *1*, 20.
[3] Tanaka, K.; Takahara, A.; Kajiyama, T. *Macromolecules* **1998**, *31*, 863.
[4] Lee, H.; Archer, L. A. *Macromolecules* **2001**, *34*, 4572.
[5] Lee, H.; Archer, L. A. *Polymer* **2002**, *43*, 2721.
[6] Wang, Z.-W.; Wang, P.-L.; Hu, C.-Y. *Packag. Technol. Sci.* **2012**, *25*, 329.
[7] Gillet, G.; Vitrac, O.; Desobry, S. *Ind. Eng. Chem. Res.* **2010**, *49*, 7263.
[8] Ferrara, G.; Bertoldo, M.; Scoponi, M.; Ciardelli, F. *Polym. Degrad. Stabil.* **2001**, *73*, 411.
[9] Bertoldo, M.; Ciardelli, F.; Ferrara, G.; Scoponi, M. *Macromol. Chem. Phys.* **2003**, *204*, 1869.
[10] Alin, J.; Hakkarainen, M. *J. Appl. Polym. Sci.* **2010**, *118*, 1084.
[11] Bertoldo, M.; Ciardelli, F. *Polymer* **2004**, *45*, 8751.
[12] MacElroy, J. M. D.; Boyle, M. J. *Chem. Eng. J.* **1999**, *74*, 85.
[13] Skoulidas, A. I.; Bowen, T. C.; Doelling, C. M.; Falconer, J. L.; Noble, R. D.; Sholl, D. S. *J. Membrane Sci.* **2003**, *227*, 123.
[14] Ahn, W.-Y.; Kalinichev, A. G.; Clark, M. M. *J. Membrane Sci.* **2008**, *309*, 128.
[15] Russell, R. J.; Axel, A. C.; Shields, K. L.; Pishko, M. V. *Polymer* **2001**, *42*, 4893.
[16] Bemporad, D.; Essex, J. W.; Luttmann, C. *J. Phys. Chem. B* **2004**, *108*, 4875.
[17] Xiang, T.-X.; Anderson, B. D. *Adv. Drug Deliver. Rev.* **2006**, *58*, 1357.
[18] Murad, S. *J. Chem. Phys.* **2011**, *134*, 114504.
[19] Bernardo, G. *J. Polym. Res.* **2012**, *19*, 9836.
[20] Zhu, S. Q.; Welsh, N.; Hirt, D. E. *J. Plast. Film. Sheet.* **2007**, *23*, 187.
[21] Limm, W.; Hollifield, H. C. *Food Addit. Contam.* **1996**, *13*, 949.
[22] Brandsch, J.; Mercea, P.; Rüter, M.; Tosa, V.; Piringer, O. *Food Addit. Contam.* **2002**, *19* (Supplement), 29.
[23] Vittoria, V. *J. Mater. Sci.* **1995**, *30*, 3954.
[24] Wang, Z.-W.; Wang, P.-L.; Hu, C.-Y. *Packag. Technol. Sci.* **2010**, *23*, 457.
[25] Reynier, A.; Dole, P.; Humbel, S.; Feigenbaum, A. *J. Appl. Polym. Sci.* **2001**, *82*, 2422.
[26] Chae, K.; Elvati, P.; Violi, A. *J. Phys. Chem. B* **2011**, *115*, 500.
[27] Datla, V. M.; Shim, E.; Pourdeyhimi, B. *J. Appl. Polym. Sci.* **2011**, *121*, 1335.
[28] Williams, J. B.; Geick, K. S.; Falter, J. A.; Hall, L. K. *J. Vinyl Addit. Technol.* **1995**, *1*, 282.
[29] Shimada, K.; Kato, H.; Saito, T.; Matsuyama, S.; Kinugasa, S. *J. Chem. Phys.* **2005**, *122*, 244914.
[30] Szefczyk, B.; Cordeiro, M. N. D. S. *J. Phys. Chem. B* **2011**, *115*, 3013.
[31] von Meerwall, E.; Waheed, N.; Mattice, W. L. *Macromolecules* **2009**, *42*, 8864.

[32] Mansfield, K. F.; Theodorou, D. N. *Macromolecules* **1991**, *24*, 4295.
[33] Sajkiewicz, P.; Gradys, A.; Ziabicki, A.; Misztal-Faraj, B. *E-Polymers* **2010**, no. 124.
[34] Hofman, D.; Ulbrich, J.; Fritsch, D.; Paul, D. *Polymer* **1996**, *37*, 4773.
[35] Han, J.; Boyd, R. H. *Polymer* **1996**, *37*, 1797.
[36] Bharadwaj, R. K.; Boyd, R. H. *Polymer* **1999**, *40*, 4229.
[37] Cuthbert, T. R.; Wagner, N. J.; Paulaitis, M. E.; Murgia, G.; D'Aguanno, B. *Macromolecules* **1999**, *32*, 5017.
[38] Logotheti, G. E.; Theodorou, D. N. *Macromolecules* **2007**, *40*, 2235.
[39] *LAMMPS Molecular Dynamics Simulator*. http://lammps.sandia.gov.
[40] Nosé, S. *J. Chem. Phys.* **1984**, *81*, 511.
[41] Tuckerman, M.; Berne, B. J.; Martyna, G. J. *J. Chem. Phys.* **1992**, *97*, 1990.
[42] Humphrey, W.; Dalke, A.; Schulten, K. *J. Mol. Graphics* **1996**, *14*, 33.
[43] Jorgensen, W. L.; Maxwell, D. S.; Tirado-Rives, J. *J. Am. Chem. Soc.* **1996**, *118*, 11225.
[44] Saiz, L.; Padró, J. A.; Guárdia, E. *J. Chem. Phys.* **2001**, *114*, 3187.
[45] MacKerell, A. D., Jr.; Bashford, D.; Bellott, M.; Dunbrack, R. L., Jr.; Evanseck, J. D.; Field, M. J.; Fischer, S.; Gao, J.; Guo, H.; Ha, S.; Joseph-McCarthy, D.; Kuchnir, L.; Kuczera, K.; Lau, F. T. K.; Mattos, C.; Michnick, S.; Ngo, T.; Nguyen, D. T.; Prodhom, B.; Reiher, W. E., III; Roux, B.; Schlenkrich, M.; Smith, J. C.; Stote, R.; Straub, J.; Watanabe, M.; Wiórkiewicz-Kuczera, J.; Yin, D.; Karplus, M. *J. Phys. Chem. B* **1998**, *102*, 3586.
[46] Zhu, X.; Lopes, P. E. M.; MacKerell, A. D., Jr. *WIREs Comput. Mol. Sci.* **2012**, *2*, 167.
[47] Luty, B. A.; Tironi, I. G.; van Gunsteren, W. F. *J. Chem. Phys.* **1995**, *103*, 3014.
[48] Davies, J. T.; Rideal, E. K. *Interfacial Phenomena*, 2nd Ed., Academic Press, New York, **1977**, Vol. 2.
[49] Perez, M.; Lame, O.; Leonforte, F.; Barrat, J.-L. *J. Chem. Phys.* **2008**, *128*, 234904.
[50] Matsuura, H.; Fukuhara, K. *J. Mol. Struct.* **1985**, *126*, 251.
[51] Yoshida, H.; Takikawa, K.; Kaneko, I.; Matsuura, H. *J. Mol. Struct.* (*Theochem*) **1994**, *311*, 205.
[52] Bulacu, M.; van der Giessen, E. *J. Chem. Phys.* **2005**, *123*, 114901.

(Cheng, F.)

